A yttrium aluminosilicate glass-ceramic to join SiC/SiC composites

Journal of the European Ceramic Society 44 (2024) 3579–3587

Contents lists available at ScienceDirect

Journal of the European Ceramic Society

journal homepage: www.elsevier.com/locate/jeurceramsoc

# A yttrium aluminosilicate glass-ceramic to join SiC/SiC composites

Carla Malinverni [a,*], Milena Salvo [a], Maciej Ziętara [b], Grzegorz Cempura [b], Adam Kruk [b], Jonathan Maier [c], Calvin Prentice [d], Michael Farnham [d], Valentina Casalegno [a]

[a] Department of Applied Science and Technology, Politecnico di Torino, Corso Duca degli Abruzzi 24, 10129 Torino, Italy
[b] International Centre of Electron Microscopy for Materials Science, AGH University of Krakow, al. A. Mickiewicza 30, 30-059 Krakow, Poland
[c] Fraunhofer Institute for Silicate Research ISC, Center for High Temperature Materials and Design HTL, Neunerplatz 2, 97082 Würzburg, Germany
[d] Archer Technicoat Ltd, ATL, Unit E, Progress Road, High Wycombe, Bucks HP12 4JD United Kingdom

ARTICLE INFO

*Keywords:*
Joining
Glass-ceramic
Composites
SiC/SiC
Yttrium aluminosilicate

ABSTRACT

In this work, a yttrium aluminosilicate glass-ceramic was employed to join two different SiC/SiC ceramic matrix composites to be used as radiant tube furnace components for energy-intensive industries, such as steelmaking. Two different joining processes are reported. The joints were morphologically characterized using scanning electron microscopy, and they were mechanically tested using the single-lap offset shear test at room temperature, where the failure was caused by the delamination of the composite, thus denoting an excellent adhesion between the glass-ceramic and the SiC/SiC composite.

## 1. Introduction

Extreme operating environments are conditions which require specific materials that are designed to withstand them. Non-oxide-based ceramic matrix composites (CMCs) are high-performance materials that have been successfully used in harsh conditions, like high temperatures and corrosive environments [1,2], and for several applications such as aerospace, gas turbines [3,4], as well as nuclear energy applications [5–7]. For the joining of these composites, different solutions have been proposed in the course of the years, for example by using brazing alloys [8,9], MAX phase materials (M: transition metal, A: A-group element, X: C or N) such as $Ti_3SiC_2$ in forms of tape, synthetized powders or pre-sintered powders [10], preceramic polymers [11], as well as glass-ceramics [12]. In ref. [13], several glass-ceramic systems that were used for this purpose are illustrated. Within these systems, yttrium aluminosilicate (YAS) systems have been proposed as coating materials for non-oxide-based substrates for high temperatures applications [14,15], where different phenomena can occur like oxidation [16], erosion [17], corrosion and volatilization by water vapour that can cause surface recession [18]. YAS ($Y_2O_3$-$Al_2O_3$-$SiO_2$) glass-ceramics have also been the subject of interest for their excellent properties as environmental barrier coatings (EBCs) [19–21], where they are utilised to protect and join SiC-based components, and their use as glass-ceramic filler for laser-supported sealing of SiC components was also investigated [22]. Several studies were conducted on $Y_2O_3$-$Al_2O_3$-$SiO_2$ systems regarding the effect of different compositions on the crystallization behaviour [23], the modification of properties, e.g. coefficient of thermal expansion (CTE) and refractive index [24], and to investigate the effect of high temperature on the microstructure [25].

Properties of YAS systems include high electrical resistivity, chemical durability and stability, low thermal conductivity, and low coefficient of thermal expansion, comparable with that of the SiC/SiC CMCs substrates to minimize thermal stresses in the joint. These unique properties make YAS systems promising coatings and joining materials for SiC/SiC composites for high-temperature applications [26]. They are also characterized by high glass transition temperatures, hardness and elastic modules [27].

In this work, a YAS glass-ceramic was utilized as joining material for SiC/SiC CMCs to be used as radiant tubes in the steel manufacturing industry as alternatives for their metallic counterparts like stainless steel and Inconel alloys that are currently used. The basic idea is to use these high-performance, lightweight materials for high-temperature components, to replace the currently used heavy superalloys, thus enhancing energy efficiency. Fraunhofer ISC, Bayreuth, Germany produced the YAS glass system used in this work. It was initially designed and successfully used as an environmental barrier coating for SiC/SiC composites [28]. The YAS glass-ceramic is here used as joining material considering its role as EBC and, therefore, its high resistance to extreme environmental conditions. These joints are expected to withstand high operating temperatures, up to 1200 °C, and harsh conditions such as combustion

* Corresponding author.
*E-mail address:* carla.malinverni@polito.it (C. Malinverni).

https://doi.org/10.1016/j.jeurceramsoc.2023.12.095
Received 12 October 2023; Received in revised form 19 December 2023; Accepted 28 December 2023
Available online 30 December 2023

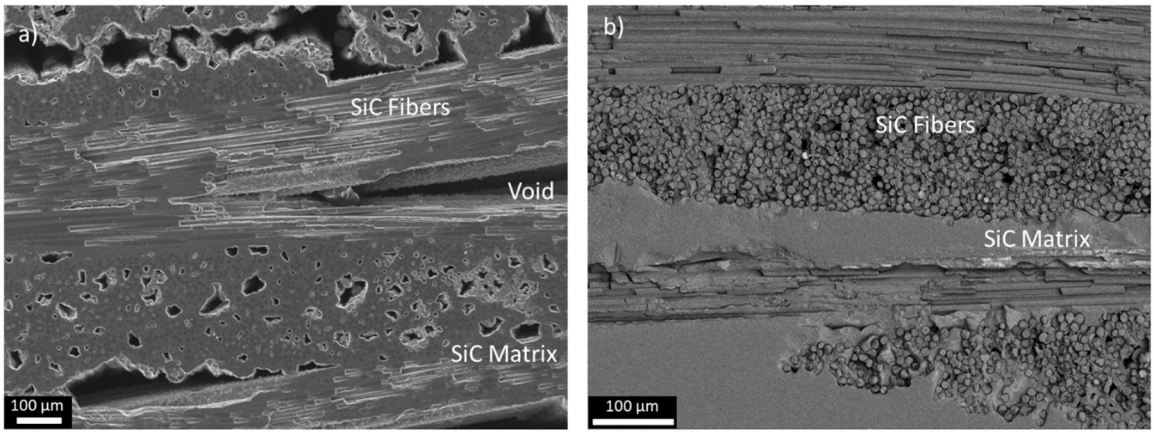


**Fig. 1.** SEM cross-sections of ATL-SiC/SiC (a), and BJS-SiC/SiC (b). SiC fibers and SiC matrix can be observed, as well as the presence of voids in the CMCs. The images are obtained with SE (Secondary Electron) detector.

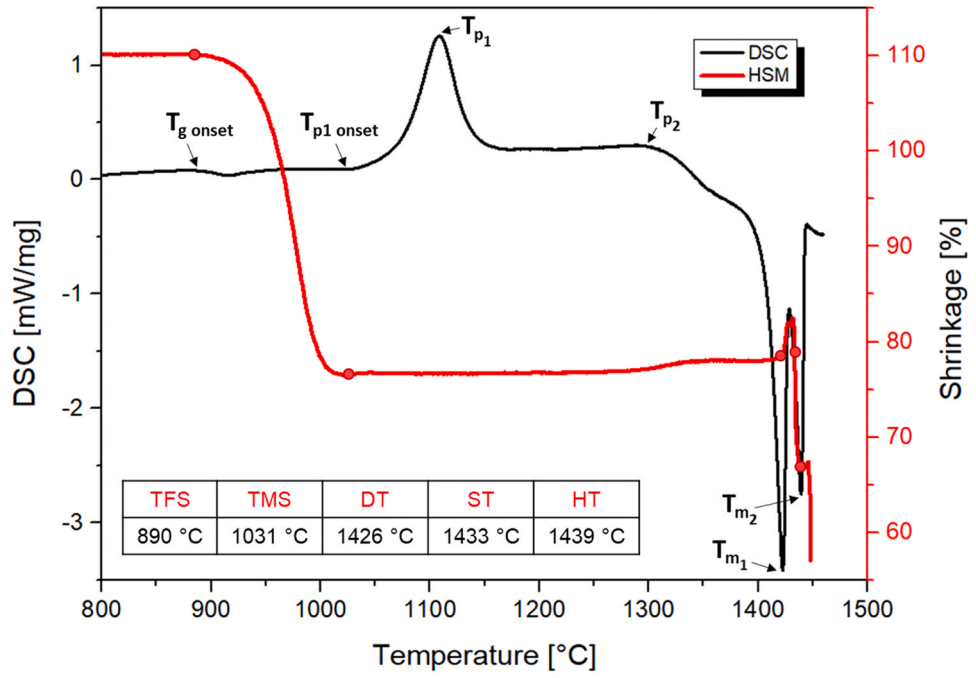


**Fig. 2.** DSC curve of the YAS glass and HSM curve of YAS glass on BJS-SiC/SiC. The characteristic temperatures from DSC are: glass transition temperature ($T_{g\ onset}$), onset of the first crystallization temperature peak ($T_{p1\ onset}$), first crystallization temperature peak ($T_{p1}$), second crystallization temperature peak ($T_{p2}$), and melting temperature ($T_{m1}$ and $T_{m2}$). The characteristic points obtained from HSM are reported: first shrinkage temperature (TFS), maximum shrinkage temperature (TMS), deformation temperature (DT), spherical temperature (ST), and hemispherical temperature (HT). Flow temperature (FT) was not detected.

environments and hydrothermal corrosion.

## 2. Materials and methods

### 2.1. Non-oxide ceramic matrix composites

Two different SiC/SiC composites were used in this work to interrogate the properties of the joining material. ATL Archer Technicoat Ltd, United Kingdom supplied the first SiC/SiC composite. The second one, Keraman® SiC/SiC, was supplied by BJS Composites GmbH, Germany. The SiC/SiC composite supplied by ATL, referred to as ATL-SiC/SiC, comprised 1st generation ceramic-grade Nicalon SiC fibers, a boron nitride interphase coating and SiC matrix deposited by Chemical Vapour Infiltration (CVI). These samples were produced with conditions that left them more porous in nature to investigate further the viscosity and infiltration properties of the joining material. The SiC/SiC composite supplied by BJS, referred to as BJS-SiC/SiC, was manufactured by the CVI process with UBE Tyranno® S fibers with an outer fiber coating of pyrolytic carbon.

Dilatometry (DIL, 402 PC, NETZSCH, Germany) was used to measure the coefficient of thermal expansion of the two CMCs. It was conducted in air from room temperature to 1000 °C with a heating rate of 5 °C/min.

### 2.2. YAS glass-ceramic as joining material

Fraunhofer ISC, Bayreuth, Germany supplied the yttrium aluminosilicate YAS glass powders. The composition compound ratio of the oxides was 26.4 wt% $SiO_2$ (>99,98 wt%, Sipur Al, Bremthaler Quarzitwerke GmbH, Germany), 33.9 wt% $Al_2O_3$ (>99,39 wt%, Fluka 06285, Honeywell International Inc., USA) and 39.7 wt% $Y_2O_3$ (>99,00 wt%, AB134552 Grade A, H.C.Starck Tungsten GmbH, Germany) for the $Y_2O_3$-$Al_2O_3$-$SiO_2$ system. The oxide powders were mixed and melted

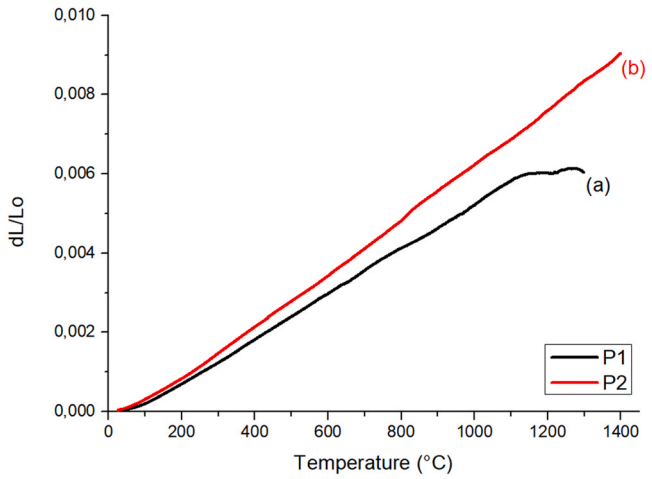


**Fig. 3.** Dilatometric curves of the YAS glass-ceramics obtained from the two joining processes, P1 (a) and P2 (b).

together. The melt was then poured into moulds and cooled. The resulting glass was milled with a vibrating cup mill (pulverisette 9, FRITSCH GmbH - Milling and Sizing, Germany). In the following, the glass powder will be called YAS glass.

The YAS glass powders were characterized using differential scanning calorimetry (DSC 404 F3 Pegasus, NETZSCH, Germany) and heating-stage microscopy (HSM, Hesse Instruments, Germany) equipped with an image analysis system (EM 301, Hesse Instruments, Germany). DSC was carried out on the YAS system under flowing Ar, from room temperature to 1450 °C, with a heating rate of 10 °C/min. In order to investigate the shrinkage of the glass pellet as a function of the temperature on the CMC, HSM of a YAS glass pellet (around 3 mm of diameter) placed on a SiC/SiC plate was performed from room temperature to 1450 °C, with a heating rate of 10 °C/min, under flowing Ar. X-ray diffraction (XRD) was conducted to identify the crystalline phases of the YAS glass-ceramic present after the joining processes with the use of Malvern PANalytical X'Pert PRO diffractometer with the support of X-Pert HighScore software, as well as two other measurement devices D5005, Siemens AG, Germany, and SmartLab, Rigaku, Japan, with SmartLab Studio II software.

The joining procedure consisted of preparing a slurry containing YAS glass powders (70 vol%) and ethanol (30 vol%). The glass slurry was deposited with a spatula onto a SiC/SiC substrate, and another SiC/SiC substrate was subsequently placed on top and pressed lightly to maximize the area in contact with the slurry. Based on the composite's surface chosen to be joined, two different configurations of joints were performed: flat-joint, where the composite's weave was parallel to the joined surface, and butt-joint, characterized by having fibers' bundles perpendicular to the joining area. In the first case, it was possible to study the interface between the glass ceramic and the matrix. In contrast, in the second case, it was possible to investigate the infiltration of the glass ceramic along the fibers. After preparing the samples, they were subjected to a specific thermal treatment to obtain the joints in a tubular furnace (STF 16/180, Carbolite, Hope Valley, United Kingdom) under a continuous flow of Ar. In this work, two joining processes were studied based on the result of DSC and HSM analyses, and they were performed with a heating rate of 10 °C/min. The first joining process, identified as P1, consisted of 1400 °C, 30 min, followed by 1105 °C, 60 min under flowing Ar, with a cooling rate of 10 °C/min. The second joining process, identified as P2, consisted of 1450 °C, 20 min, followed by 1105 °C, 60 min under flowing Ar. For this second joining process, the cooling rate to reach room temperature was 8 °C/min, which was chosen to have a slower cooling to limit and avoid the formation of porosities in the glass-ceramic layer. Moreover, for the P2 joining process, a tungsten weight (1.2 kPa) was placed on top of the joints during the joining process in the tubular furnace to promote adhesion with the CMC substrates. Dilatometry was used to measure the coefficient of

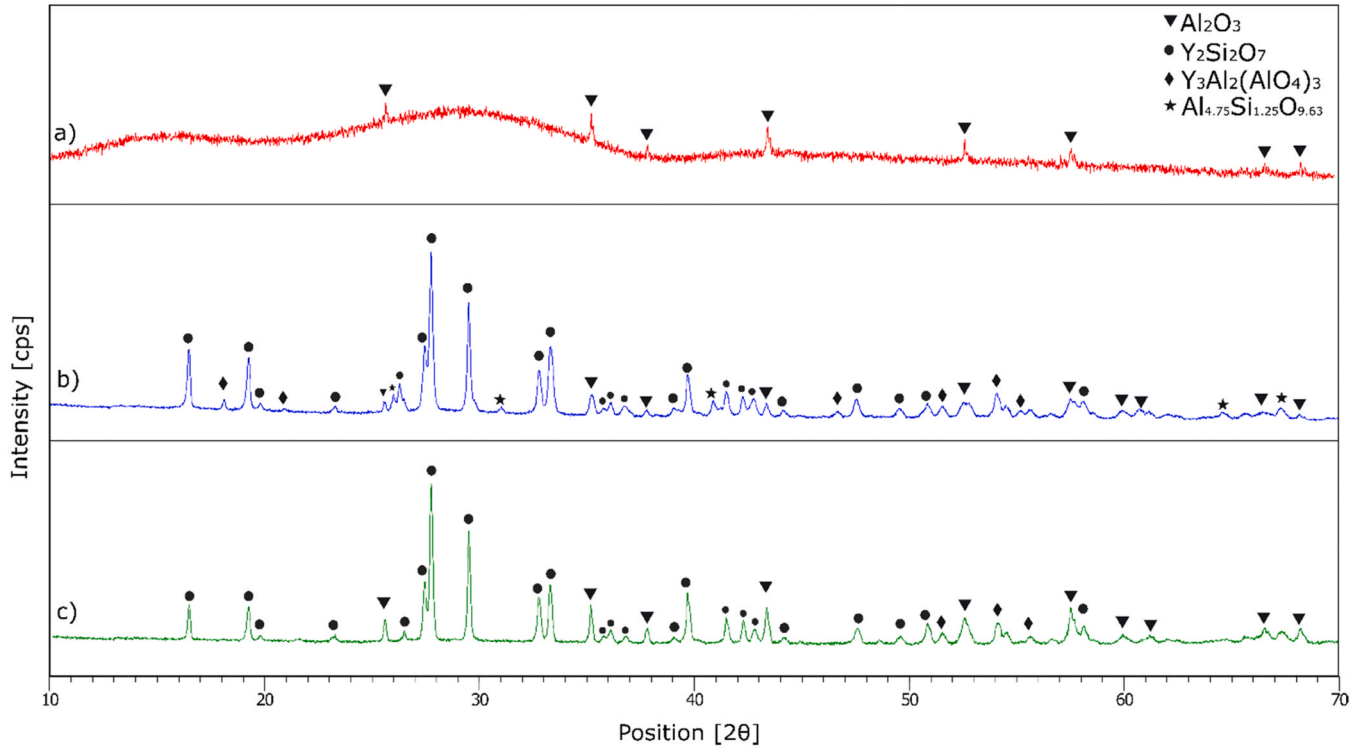


**Fig. 4.** XRD patterns of the YAS glass (a), YAS glass-ceramic obtained with the P1 thermal treatment (b) and YAS glass-ceramic obtained with the P2 thermal treatment (c). $Al_2O_3$: PDF card n. 01–076-0144; $Y_2Si_2O_7$: PDF card n. 00–038-0440; $Y_3Al_2(AlO_4)_3$: PDF card n. 01–082-0575; $Al_{4.75}Si_{1.25}O_{9.63}$: PDF card n. 01–079-1454.

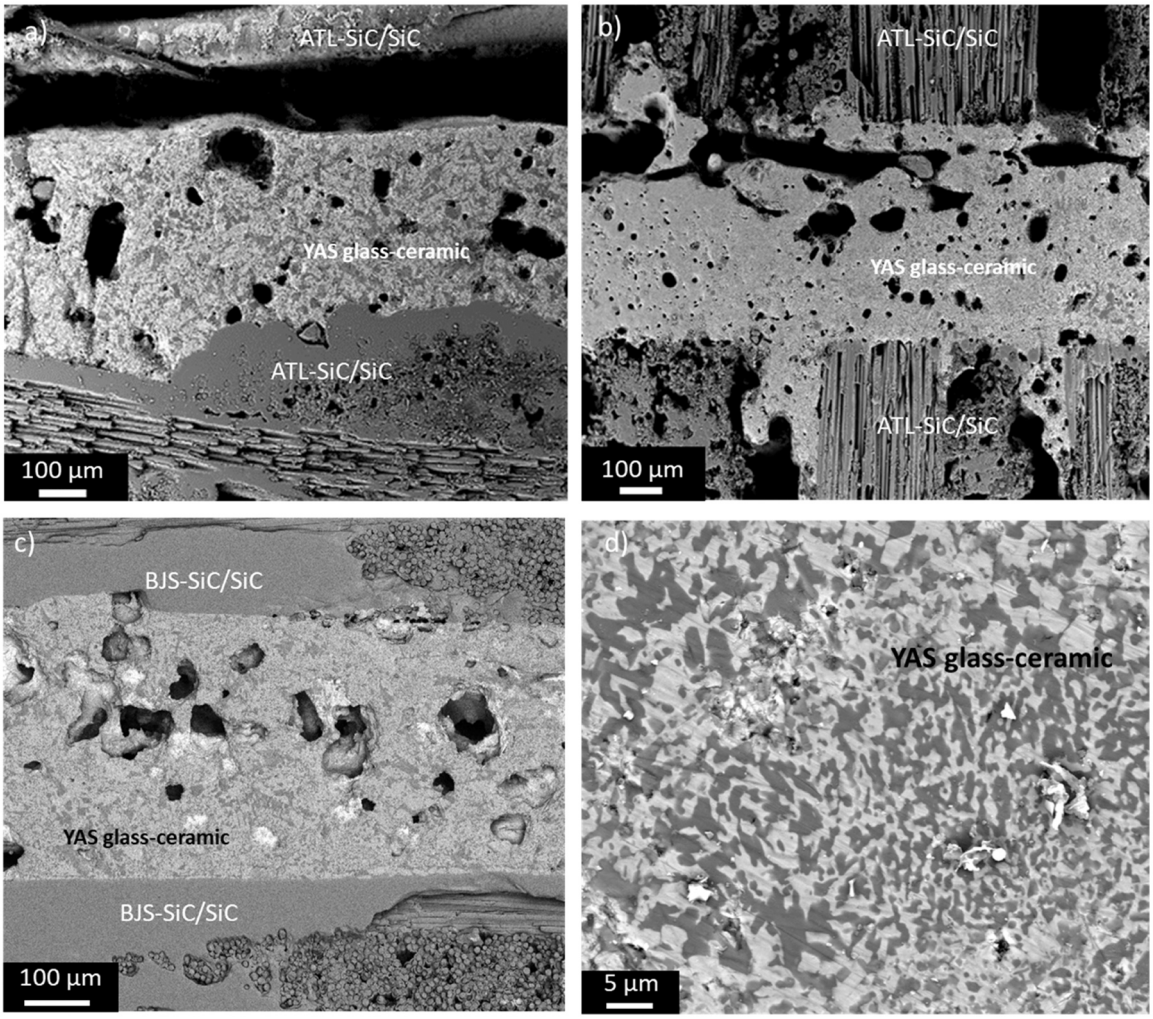


**Fig. 5.** FE-SEM images of the cross-sectioned ATL-SiC/SiC joined with YAS in (a) flat-joint, (b) butt-joint configuration, and of the cross-sectioned BJS-SiC/SiC joined with YAS in (c) flat-joint configuration, and the microstructure obtained (d) after P1. These joints are obtained at 1400 °C for 30 min, followed by a heat treatment at 1105 °C for 60 min (P1). The images are obtained in BSE (Back-Scattered Electrons) mode.

thermal expansion and the dilatometric softening point of the YAS glass-ceramics obtained with the two different joining processes. It was conducted in air from room temperature to 1400 °C with a heating rate of 5 °C/min.

The morphological and compositional characterization of the YAS glass-ceramic joints was conducted using scanning electron microscopy (SEM, JCM-6000Plus, JEOL), as well as high-resolution scanning electron microscopy MERLIN with the GEMINI II column and Schottky Field Emission Gun electron source (FE-SEM, MERLIN Gemini II, ZEISS, Germany) equipped with an energy-dispersive X-ray spectroscopy (EDX) microanalysis system for elemental mapping.

Single-lap offset (SLO) tests were performed to measure the apparent shear strength of the joints, where the dimensions of the tested composites were 10 mm × 15 mm for ATL-SiC/SiC and 10 mm × 10 mm for BJS-SiC/SiC. SLO tests were conducted at room temperature on a universal testing machine (SINTEC D/10), with a crosshead speed of 0.5 mm/min and a 50 kN load cell. A schematic representation of this test can be found in reference [29]. At least three samples were tested for each joint obtained using different SiC/SiC. All the fracture surfaces were observed and macroscopically characterized; the results of the mechanical tests were expressed as mean ± standard deviation. X-ray computed tomography (CT-scan, Fraunhofer IKTS, Germany) characterized by an open microfocus X-ray tube (filament voltage 180 kV, current 90 µA, exposure time 1 s, 0.2 mm Cu filter), was performed on a YAS glass-ceramic BJS-SiC/SiC flat-joint, obtained with the joining process P2, to have a 3D representation of the typical joint obtained. In particular, to detect the eventual presence of defects at the CMC/YAS interface and the level of porosity in the glass-ceramic layer.

## 3. Results and discussion

The cross-sections of SiC/SiC composites supplied by ATL and BJS are shown in Fig. 1a-b, respectively.

From the SEM images, the weave pattern of the fibers can be noticed. The composite supplied by ATL appeared to be more porous, as expected, with voids present both around the fibers bundles and slightly around the fibers themselves, while the BJS composite seemed less porous, and the porosities were mainly localized around the fibers bundles. The dilatometric analysis showed that the CTE of ATL-SiC/SiC is 5.2 $\cdot 10^{-6}$ °C$^{-1}$ (200 °C – 600 °C), while the CTE of BJS-SiC/SiC is 5.4$\cdot 10^{-6}$ °C$^{-1}$ (200 °C – 600 °C).

The characteristic temperatures of the YAS glass were obtained from DSC and HSM analyses and the curves are reported in Fig. 2. They were used for identifying the appropriate joining processes.

The DSC analysis showed that the glass transition temperature ($T_{g\ onset}$) is 892 °C, while the first crystallization peak, $T_{p1,}$ is 1105 °C. A less intense exothermic peak at around 1300 °C was associated with a second crystallization event ($T_{p2}$). Furthermore, two endothermic peaks at

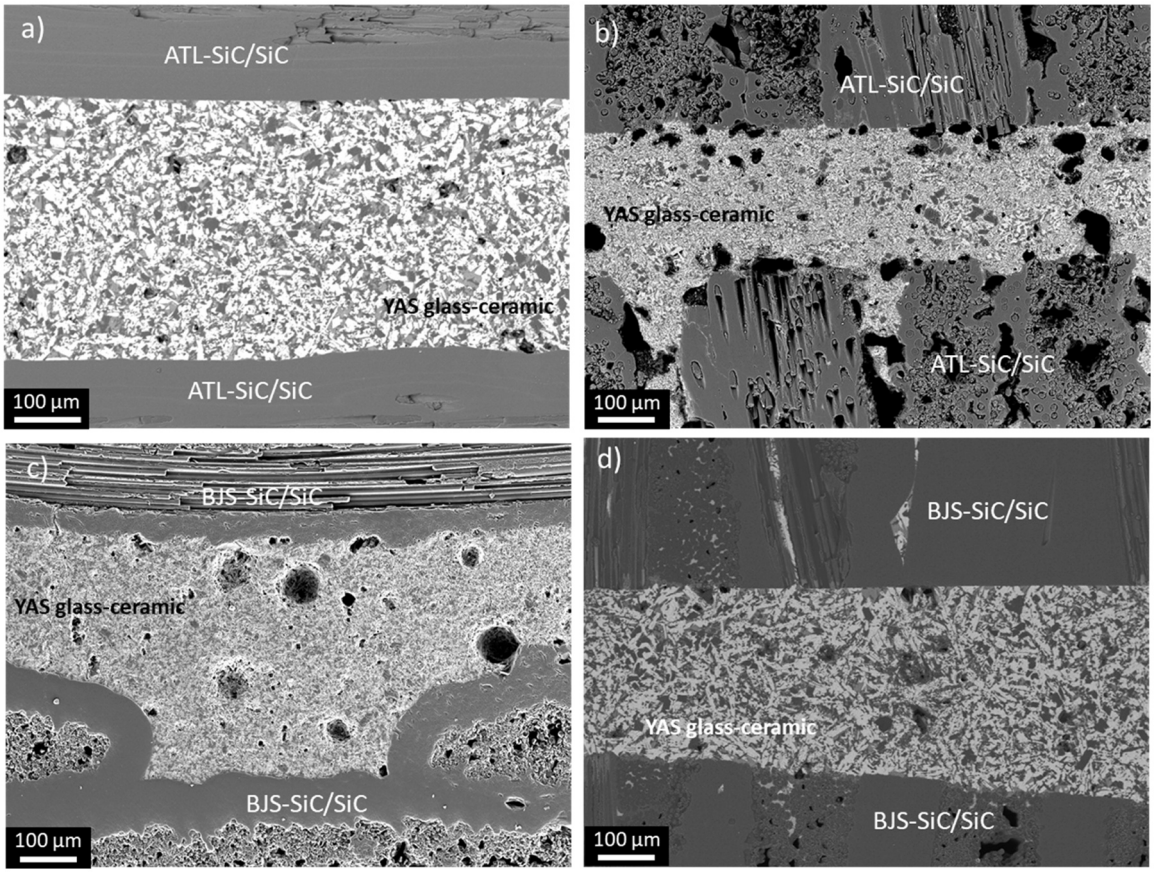


**Fig. 6.** FE-SEM cross-sections of ATL-SiC/SiC joined with YAS in (a) flat-joint and (b) butt-joint configuration, and of the cross-sectioned BJS-SiC/SiC joined with YAS in (c) flat-joint and (d) butt-joint configuration. These joints are obtained with joining process P2. Images a, b and d are obtained in BSE mode, while image c is obtained with SE detector.

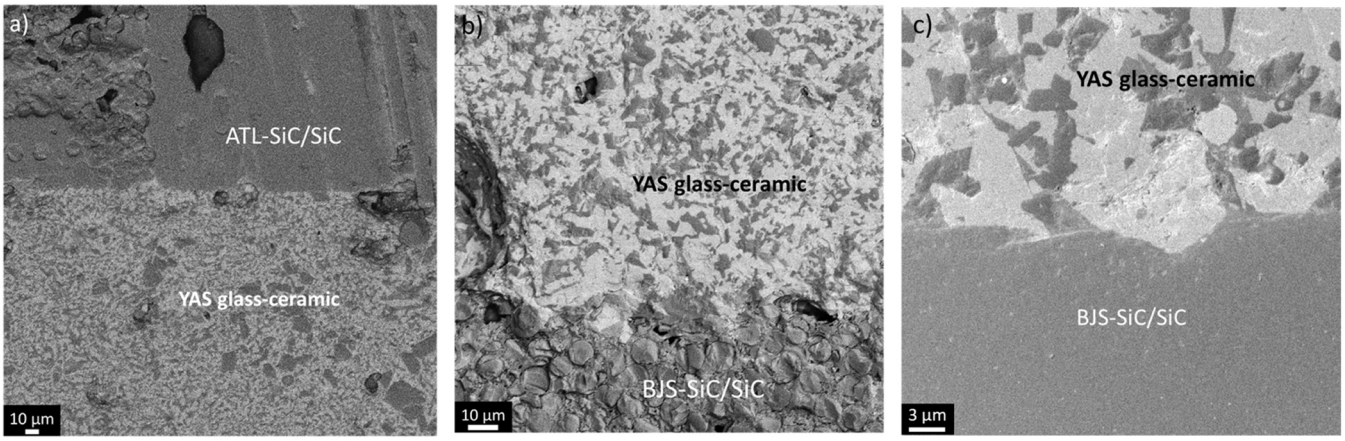


**Fig. 7.** FE-SEM images showing the interface of the YAS glass-ceramic with the ATL-SiC/SiC (a) butt-joint and BJS-SiC/SiC (b) flat-joint. Image (c) shows the interface between the matrix of BJS-SiC/SiC and the glass-ceramic. The images are obtained in BSE mode.

1422 °C ($T_{m1}$) and 1439 °C ($T_{m2}$) were found. To evaluate the sintering behaviour, HSM analysis of a YAS glass powder pellet was performed on BJS-SiC/SiC. The characteristic temperatures obtained were: first shrinkage temperature (TFS) at 890 °C, where the initial shrinkage takes place; maximum shrinkage temperature (TMS) at 1031 °C, deformation temperature (DT) at 1426 °C, spherical temperature (ST) at 1433 °C and hemispherical temperature (HT) at 1439 °C. From the HSM analysis performed, an expansion was found at a temperature slightly above 1400 °C; a similar behaviour was observed by Garcia et al. [2]. This swelling event was also observed when performing the HSM of YAS glass on a different substrate, i.e. alumina substrate. A comparison of the HSM data with the DSC data shows that the onset of crystallization temperature for the first peak ($T_{p1\ onset}$), around 1027 °C, is very close to the maximum shrinkage temperature TMS, indicating that the sintering and crystallization processes are not independent, but their competition (represented by the sinterability parameter, which is around −4 °C) causes an excessive surface crystallization before the completion of the sintering process, which reduces the viscous flow and forms a porous

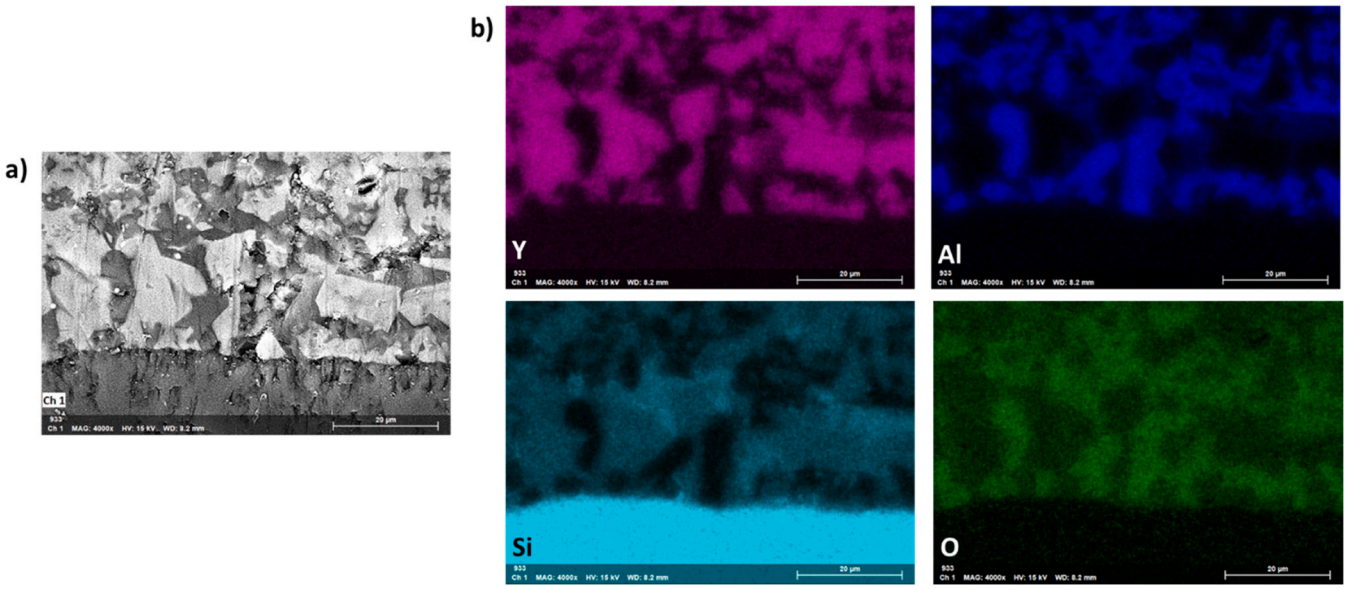


**Fig. 8.** EDX elemental maps of YAS/CMC interface of ATL-SiC/SiC in flat-joint configuration obtained with joining process P2; (a) shows a high-resolution image of the area of interest, while (b) reports the elemental maps of Y, Al, Si and O.

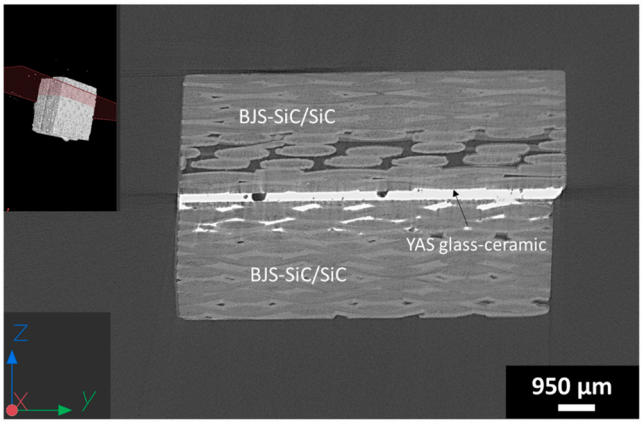


**Fig. 9.** CT-Scan of BJS-SiC/SiC flat-joint with YAS glass-ceramic obtained after the joining process P2. The infiltration of the glass-ceramic into the SiC/SiC composite can be observed.

glass-ceramic.

Based on these analyses, two thermal treatments were chosen to process the CMC's YAS joining. The first joining process, P1, was carried out at 1400 °C (after the second crystallization peak and before the start of the expansion and the melting) for 30 min, followed by a heat treatment at 1105 °C ($T_{p1}$) for 60 min. The second joining process, P2, was carried out at 1450 °C, above the melting temperature, for 20 min, followed by a treatment at 1105 °C for 60 min.

The curves from dilatometric analysis of the YAS glass-ceramics obtained with the two joining processes P1 and P2 are shown in Fig. 3.

The CTE of the YAS glass-ceramic obtained with the P1 is 5.7 $\cdot 10^{-6}$ °C$^{-1}$ (200 °C – 600 °C) and the dilatometric softening temperature is around 1275 °C, while for the samples obtained with the P2, the coefficient was 6.3 $\cdot 10^{-6}$ °C$^{-1}$ (200 °C – 600 °C) and the softening was not detected up to 1400 °C. The excellent matching of the coefficient of thermal expansion of the composites and the YAS glass-ceramics, together with their high softening points, make them promising materials to join SiC/SiC for the high temperatures and corrosive environments that are found in the steelmaking industry.

Furthermore, XRD measurements were carried out on the YAS glass (Fig. 4a) as well as on the YAS glass-ceramics obtained with P1 and P2 thermal treatments (Fig. 4b-c).

The XRD pattern of the YAS glass showed a broad band confirming the mainly amorphous nature of the YAS powder. The peaks present are due to alumina which crystallized during the solidification of the YAS melt.

Concerning the XRD patterns of the glass-ceramics, yttrium disilicate (β-$Y_2Si_2O_7$) was found to be the main phase in the YAS glass-ceramics and $Al_2O_3$ was also present after both thermal treatments, P1 and P2. In addition, mullite and YAG ($Y_3Al_2(AlO_4)_3$) were found as further phases in the YAS glass-ceramic after P1, while there were only small amounts of YAG and no mullite in the YAS obtained with P2. The heat treatment at a temperature above the melting point, followed by the cooling down to the $T_{p1}$, drastically reduced the nucleation and growth of the secondary phases, and the first exothermic peak of the DSC curve (Fig. 2) can be associated with the crystallization of $Y_2Si_2O_7$.

The joining process P1 was performed with SiC/SiC in both flat-joint and butt-joint configurations. Fig. 5 shows the cross-sections of an ATL-SiC/SiC joined sample in the flat-joint configuration (Fig. 5a), and in the butt-joint configuration (Fig. 5b). The cross-section of a BJS-SiC/SiC joined sample in the flat-joint configuration (Fig. 5c) and the typical YAS microstructure obtained (Fig. 5d) are also reported.

As can be observed from the FE-SEM images, the interface between the glass-ceramic and the composites is not continuous, and detachments are visible at the upper interface, especially with the ATL-SiC/SiC. Furthermore, a significant number of pores, with irregular shapes and dimensions, were present within the glass-ceramic layer, which can negatively affect the mechanical strength of the joined components. As previously mentioned, the remarkably low sinterability parameter in the YAS system leads to premature surface crystallization before the sintering process is fully complete. This premature crystallization hampers viscous flow, resulting in the formation of a porous glass-ceramic structure and a very limited infiltration of the composite surface, particularly at the upper interface.

To limit the formation of pores within the glass-ceramic and to improve its infiltration and adhesion at the YAS/CMC interface, other joined samples were produced at a temperature above the melting point (joining process P2) placing a tungsten weight (1.2 kPa) on the joints during the process. The P1 joining process omitted the use of an external load to streamline the experimental route, yet yielded unsatisfactory results. As a consequence, higher joining temperature of P2 was paired

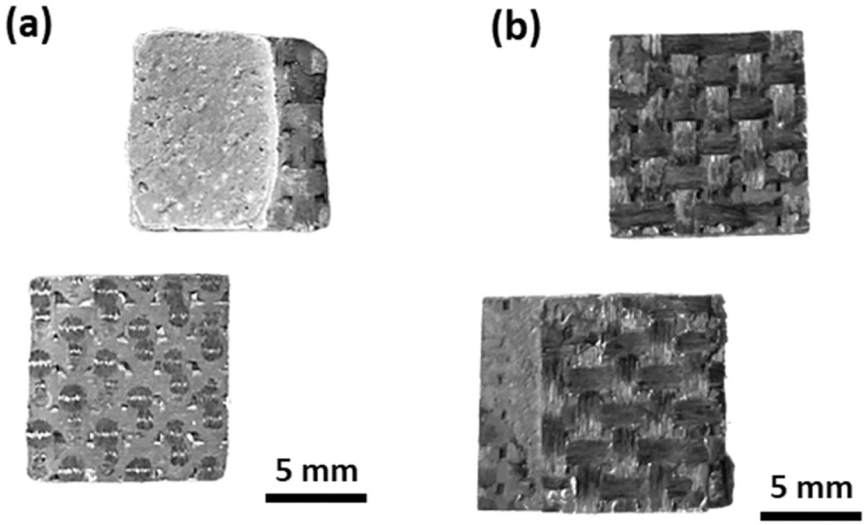


**Fig. 10.** Typical fracture surfaces of YAS glass-ceramic BJS-SiC/SiC flat-joints, obtained with joining process P1 (a) and P2 (b), after single lap offset shear tests. An adhesive fracture was observed for the joints obtained with P1, while the delamination of the SiC/SiC composite on the joining area can be observed for the joints obtained with P2.

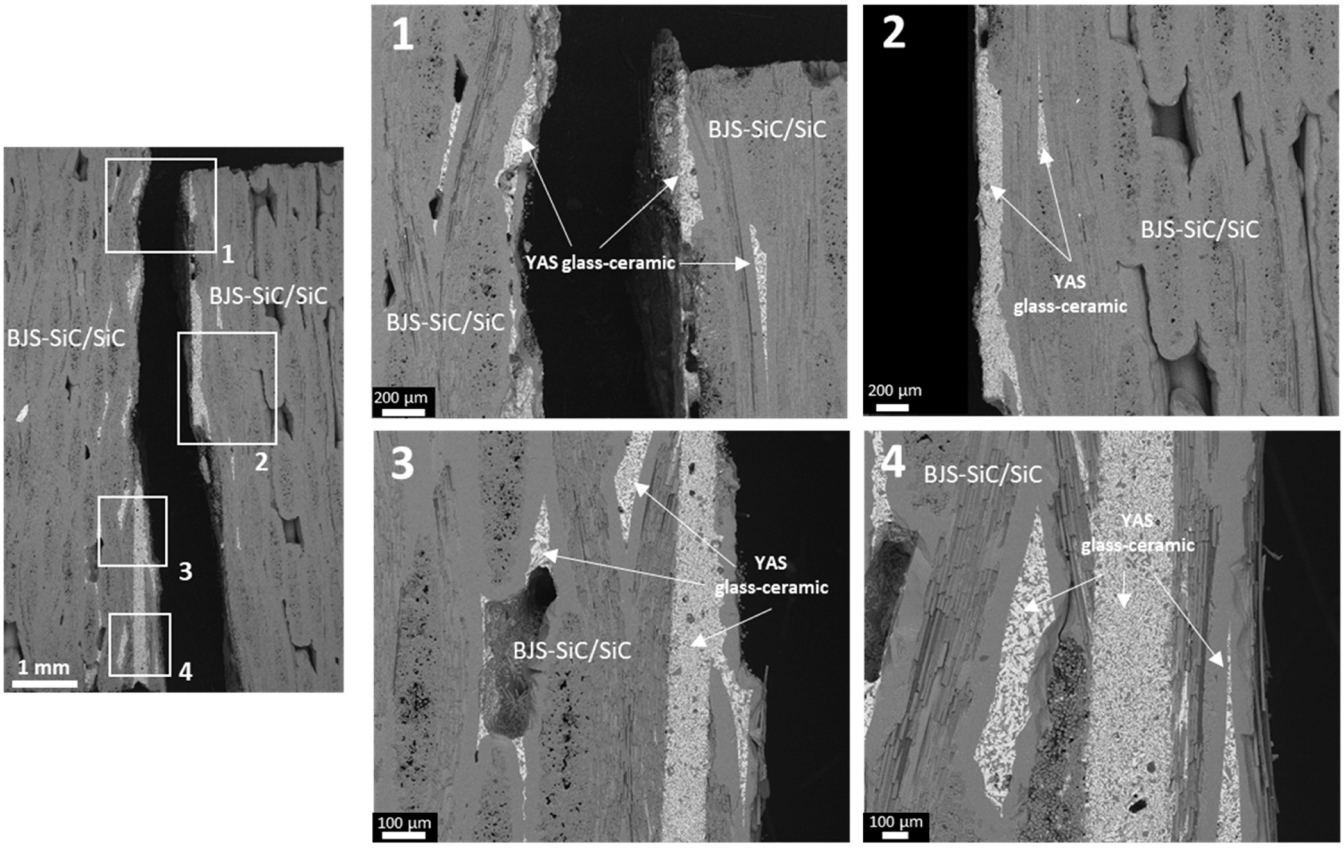


**Fig. 11.** FE-SEM cross-sections of fracture surfaces of YAS glass-ceramic BJS-SiC/SiC flat-joint, obtained with joining process P2, after performing SLO shear tests. It is possible to notice the infiltration of the glass-ceramic into the SiC/SiC composite and the failure mode that occurred after shear testing, caused by the delamination of the CMC.

with employing a tungsten weight on the top of the sample to enhance the adhesion under minimal external pressure. The cross-sections of the joints obtained with the P2 process are shown in Fig. 6. The average thickness of the glass-ceramic layer was around 200–400 µm.

For the flat configuration (Fig. 6a,c), the adhesion of the glass-ceramic at the interface with both the SiC/SiC composites was much improved, no cracks were visible and the YAS showed a homogeneous microstructure and low porosity. Concerning the butt-joints (Fig. 6b,d), the infiltration of the glass-ceramic along the fibers can be noticed and it is much more evident in the ATL-SiC/SiC, probably because of its more irregular surface, and caused a larger porosity in the YAS for these samples. Fig. 7 shows the interface between the YAS glass-ceramic and

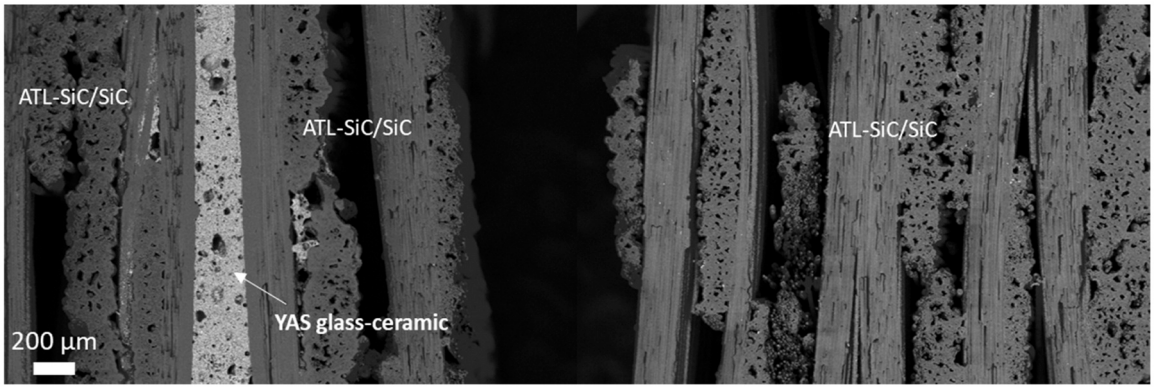


**Fig. 12.** FE-SEM cross-section of fracture surfaces of YAS glass-ceramic ATL-SiC/SiC flat-joint, obtained with joining process P2, after performing SLO shear tests. The failure was caused by the delamination of the CMC.

both the ATL-SiC/SiC butt-joint (Fig. 7a) and the BJS-SiC/SiC flat-joint (Fig. 7b). The images reveal the good wettability of the composite by the glass-ceramic, and the homogeneous microstructure of the YAS, as it can be observed at the interface with the SiC/SiC matrix (Fig. 7c).

EDX elemental mapping was performed at the interface YAS/CMC of flat-joint ATL-SiC/SiC, Fig. 8. The results confirmed the results of the XRD analysis; the darker grains in Fig. 8a can be attributed to the aluminium oxide, while the bright grey grains are $Y_2Si_2O_7$. These two crystalline regions are surrounded by an amorphous residual phase rich in silicon and aluminium oxides.

YAS glass-ceramic BJS-SiC/SiC flat-joint obtained with the P2 joining process was analyzed by X-ray computed tomography, which is reported in Fig. 9. As can be observed, the glass-ceramic significantly infiltrated into the lower SiC/SiC substrate of the joint after treatment for around 950 µm, which is promoted by the placing of the tungsten weight on the joint during the treatment.

The CT-scan allowed to visualize the joined interfaces and to detect pores or lack of joining material derived from the partially unsuccessful joining process. The soundness of the joints has been confirmed, even if pores, as already observed by SEM, have been detected in the joined specimens. Moreover, the computer-assisted tomographic analysis revealed that the joining material was confined to the interfacial area and did not flow on the side of the facing samples.

Shear tests in single-lap offset configuration were performed on BJS-SiC/SiC flat-joints produced with both joining processes. As expected from the results of the morphological analysis, the samples produced with the P1 process showed very low mechanical strength (the apparent shear strength measured was only 1 MPa), and an adhesive fracture was observed for the tested samples (Fig. 10a).

On the contrary, the YAS joined BJS-SiC/SiC samples produced with the P2 process showed a shear strength of 61 ± 12 MPa, which is higher than the interlaminar shear strength of these CMCs (around 30 MPa) and led to the delamination of the SiC/SiC composite (Fig. 10b). The increase of the shear strength of the composite near the composite/joining material interface, already observed in other systems, can be attributed to the partial infiltration of the glass-ceramic into the open porosity of the composite surface [30]. This infiltration results in a denser and stronger surface layer, alongside an additional mechanical bonding.

Fig. 11 shows the cross-section of the fracture surfaces of a YAS glass-ceramic BJS-SiC/SiC flat-joint obtained with joining process P2, after SLO tests. The infiltration of the YAS glass-ceramic into the BJS composite is evident and the failure mode that occurred after shear testing, which was caused by the delamination of the CMC, can be noted.

Shear tests in single-lap offset configuration were also performed on ATL-SiC/SiC flat-joints produced with joining process P2, but in this case, the apparent shear strength was 22 ± 1 MPa with delamination of the CMC. The difference in the apparent shear strength mean values is likely related to the more porous nature of the ATL-SiC/SiC composites, compared to the denser BJS-SiC/SiC, which caused the delamination of the composite at lower stress levels and in an area of the composite farther away from the joining interface, as can be observed in Fig. 12. The value of the interlaminar shear strength for ATL-SiC/SiC is not available.

Based on the above results, the joining process P2 conducted at 1450 °C for 20 min, followed by a heat treatment at 1105 °C for 60 min (heating rate of 10 °C/min and cooling rate to room temperature of 8 °C/min) under flowing Ar was selected as best joining process for the YAS joined SiC/SiC CMCs for this application. Further tests will verify the corrosion resistance of these joints in combustion environments by direct flame exposure tests up to 1200 °C.

## 4. Conclusions

Yttrium aluminosilicate glass-ceramic was used to successfully join SiC/SiC ceramic matrix composites supplied by ATL and BJS companies. Two joining processes were performed and one was optimized and selected as the most performative named P2, where the glass-ceramic obtained had a very high softening point (not detected by dilatometry up to 1400 °C) and a coefficient of thermal expansion close to the one of SiC/SiC. These joints were characterized by highly improved interface adhesion with the non-oxide substrate and a reduced amount of porosities in the glass-ceramic layer. Mechanical testing showed high apparent shear strength (61 ± 12 MPa), causing the delamination of the BJS-SiC/SiC composite.

## CRediT authorship contribution statement

**C. Malinverni:** Writing – original draft, Investigation, Data curation. **M. Ziętara:** Investigation. **G. Cempura:** Investigation. **A. Kruk:** Writing – review & editing. **J. Maier:** Resources, Investigation. **C. Prentice:** Resources. **M. Farnham:** Resources. **M. Salvo:** Writing – review & editing, Conceptualization, Supervision. **V. Casalegno:** Writing – review & editing, Conceptualization, Supervision.

## Declaration of Competing Interest

The authors declare that they have no known competing financial interests or personal relationships that could have appeared to influence the work reported in this paper.

## Acknowledgements

The research carried out to write this article was funded under the CEM-WAVE project. This project has received funding from

the European Union's Horizon 2020 research and innovation programme under grant agreement No. 958170. This document only reflects the authors' view. The European Commission is not responsible for any use that may be made of the information it contains. FE-SEM analysis was carried out thanks to funding from the European Union's Horizon 2020 research and innovation programme under grant agreement No. 823717 – ESTEEM3 (CeramECS and GlaMater). The authors would like to thank MSc. Carlotta Carrubba for her help in the research.

## References

[1] C. Jiménez, K. Mergia, M. Lagos, P. Yialouris, I. Agote, V. Liedtke, S. Messoloras, Y. Panayiotatos, E. Padovano, C. Badini, Wilhelmi, J. Barcena, Joining of ceramic matrix composites to high temperature ceramics for thermal protection systems, J. Eur. Ceram. Soc. vol. 36 (2016) 443–449.

[2] E. Garcìa, A. Nistal, F. Martìn de la Escalera, A. Khalifa, V. Sainz, M. Osendi, P. Miranzo, Thermally sprayed $Y_2O_3$–$Al_2O_3$–$SiO_2$ coatings for high-temperature protection of SiC ceramics, J. Therm. Spray. Technol. vol. 24 (2015) 185–193.

[3] R. Naslain, Design, preparation and properties of non-oxide CMCs for application in engines and nuclear reactors: an overview, Compos. Sci. Technol. vol. 64 (2004) 155–170.

[4] K. Lee, Special issue: environmental barrier coatings, Coatings vol. 10 (2020).

[5] M. Ferraris, V. Casalegno, S. Rizzo, M. Salvo, T. Van Staveren, Effects of neutron irradiation on glass ceramics as pressure-less joining materials for SiC based components for nuclear applications, J. Nucl. Mater. vol. 429 (2012) 166–172.

[6] L. Gozzelino, V. Casalegno, G. Ghigo, T. Moskalewicz, A. Czyrska-Filemonowicz, M. Ferraris, He-irradiation effects on glass-ceramics for joining of SiC-based materials, J. Nucl. Mater. vol. 472 (2016) 28–34.

[7] M. Ferraris, M. Salvo, V. Casalegno, S. Han, Y. Katoh, H. Jung, T. Hinoki, A. Kohyama, Joining of SiC-based materials for nuclear energy applications, J. Nucl. Mater. Vols. 417 (1-3) (2011) 379–382.

[8] X. Xiaoyu, D. Juanli, K. Sijie, L. Chenghua, F. Shangwu, W. Peng, C. Laifei, Z. Litong, Microstructure and properties of pressure-less joining of $SiC_f$/SiC composites by Ti–Si alloys, Ceram. Int. vol. 48 (2022) 22428–22441.

[9] J. Yang, X. Zhang, G. Ma, P. Lin, Y. Xu, T. Lin, P. He, W. Long, J. Li, Microstructural evolution and mechanical property of a $SiC_f$/SiC composite/Ni-based superalloy joint brazed with an Au-Cu-Ti filler, J. Eur. Ceram. Soc. vol. 41 (2021) 2312–2322.

[10] P. Tatarko, V. Casalegno, H. Chunfeng, M. Salvo, M. Ferraris, M. Reece, Joining of CVD-SiC coated and uncoated fibre reinforced ceramic matrix composites with pre-sintered $Ti_3SiC_2$ MAX phase using Spark Plasma Sintering, J. Eur. Ceram. Soc. vol. 36 (2016) 3957–3967.

[11] M. Wang, X. Dong, X. Tao, M. Liu, J. Liu, H. Du, A. Guo, Joining of various engineering ceramics and composites by a modified preceramic polymer for high-temperature application, J. Eur. Ceram. Soc. vol. 35 (2015) 4083–4097.

[12] M. Ferraris, M. Salvo, V. Casalegno, A. Ciampichetti, F. Smeacetto, M. Zucchetti, Joining of machined SiC/SiC composites for thermonuclear fusion reactors, J. Nucl. Mater. vol. 375 (2008) 410–415.

[13] M. Ferraris, V. Casalegno, F. Smeacetto, M. Salvo, Glass as a joining material for ceramic matrix composites: 25 years of research at Politecnico di Torino, Int. J. Appl. Glass Sci. vol. 11 (2020) 569–576.

[14] L. Sun, X. Shi, X. Liu, J. Fang, C. Liu, J. Zhang, Joining of $C_f$/SiC composites and $Si_3N_4$ ceramic with $Y_2O_3$–$Al_2O_3$–$SiO_2$ glass filler for high-temperature applications, Ceram. Int. vol. 47 (2021) 15622–15630.

[15] L. Sun, S. Wang, C. Hou, D. Wang, C. Liu, X. Zhang, J. Zhang, Microstructure, mechanical property and bonding mechanism of SiC ceramic joint using a novel $Y_2Si_2O_7$/Mullite glass-ceramic interlayer, Ceram. Int. vol. 49 (2023) 17885–17893.

[16] F. Smeacetto, M. Ferraris, M. Salvo, S. Ellacott, A. Ahmed, R. Rawlings, A. R. Boccaccini, Protective coatings for carbon bonded carbon fibre composites, Ceram. Int. vol. 34 (2008) 1297–1301.

[17] F. Smeacetto, M. Salvo, M. Ferraris, V. Casalegno, G. Canavese, T. Moskalewicz, S. Ellacott, R. Rawlings, A. Boccaccini, Erosion protective coatings for low density, highly porous carbon/carbon composites, Carbon vol. 47 (2009) 1511–1519.

[18] H. Eaton, G. Linsey, Accelerated oxidation of SiC CMC's by water vapor and protection via environmental barrier coating approach, J. Eur. Ceram. Soc. vol. 22 (2002) 2741–2747.

[19] J. Vogt, A. Nöth, Slurry-based environmental barrier coatings for silicon carbide and its composites – a straightforward approach, Ceram. Appl. vol. 8 (2020).

[20] J. Denga, B. Lu, K. Hu, H. Li, J. Wang, S. Fan, L. Zhang, L. Cheng, Interaction between Y-Al-Si-O glass-ceramics for environmental barrier coating materials and Ca-Mg-Al-Si-O melts, Ceram. Int. vol. 46 (2022) 18262–18273.

[21] M. Herrmann, S. Ahmad, W. Lippmann, H.-J. Seifert, Rare earth (RE: Nd, Dy, Ho, Y, Yb, and Sc) aluminosilicates for joining silicon carbide components, Int. J. Appl. Ceram. Technol. vol. 14 (2017) 675–691.

[22] M. Herrmann, W. Lippmann, A. Hurtado, $Y_2O_3$–$Al_2O_3$–$SiO_2$-based glass-ceramic fillers for the laser-supported joining of SiC, J. Eur. Ceram. Soc. vol. 34 (2014) 1935–1948.

[23] Q. Zheng, Y. Liu, L.M., Z. Liu, Y. Hu, X. Zhang, W. Deng, M. Wang, Crystallization behavior and IR structure of yttrium aluminosilicate glasses, J. Eur. Ceram. Soc. vol. 40 (2020) 463–471.

[24] M. Hyatt, D. Day, Glass properties in the Yttria-Alumina-Silica system, Commun. F. Am. Ceram. Soc. vol. 70 (1987) pp. C283-C287.

[25] S. Ahmad, T. Ludwig, M. Herrmann, M. Mahmoud, W. Lippmann, H. Seifert, Phase evaluation during high temperature long heat treatments in the $Y_2O_3$–$Al_2O_3$–$SiO_2$ system, J. Eur. Ceram. Soc. vol. 34 (2014) 3835–3840.

[26] L. Wang, S. Fan, H. Sun, B. Li, B. Zheng, J. Deng, L. Zhang, L. Cheng, Pressure-less joining of $SiC_f$/SiC composites by $Y_2O_3$–$Al_2O_3$–$SiO_2$ glass: microstructure and properties, Ceram. Int. vol. 46 (2020) 27046–27056.

[27] Y. Zhang, A. Navrotsky, Thermochemistry of glasses in the $Y_2O_3$–$Al_2O_3$–$SiO_2$ system, J. Am. Ceram. Soc. vol. 86 (2003) 1727–1732.

[28] A. Nöth, J. Maier, J. Vogt, F. Raether, Strategies for the development of environmental barrier coatings for high-temperature applications, CFI Ceram. Forum Int. vol. 99 (2022) E39–E44.

[29] C. Malinverni, M. Salvo, A. De Zanet, F. D'Isanto, F. Smeacetto, P. Bertrand, G. Puchas, S. Schafföner, V. Casalegno, Glass-ceramics for joining oxide-based ceramic matrix composites ($Al_2O_{3f}$/ $Al_2O_3$-$ZrO_2$) operating under direct flame exposure,", J. Eur. Ceram. Soc. vol. 43 (2023) 3621–3629.

[30] M. Salvo, V. Casalegno, S. Rizzo, F. Smeacetto, M. Ferraris, M. Merola, One-step brazing process to join CFC composites to copper and copper alloy, J. Nucl. Mater. vol. 374 (2008) 69–74.